

TEMPORAL ANALYSIS OF JET AND VORTEX ACTUATOR (JAVA) – INDUCED FLOWS

Hasan Gunes^{*1}, Sertac Cadirci¹, Francesco Baldani², Bernd Peters³, Ulrich Rist³

¹Department of Mechanical Engineering, Istanbul Technical University,
Gumussuyu, 34437 Istanbul, Turkey
E-mail*: guneshasa@itu.edu.tr

²University of Bologna, Forli, Dipartimento di Ingegneria delle Costruzioni
Meccaniche, Nucleari, Aeronautiche e di Metallurgia
Via Fontanelle 40, 47100 Forli, Italy

³Institut für Aerodynamik und Gasdynamik, Universität Stuttgart,
Pfaffenwaldring 21, D-70550 Stuttgart, Germany

ABSTRACT

A zero-net-mass flux Jet and Vortex Actuator (JaVA) device for active flow control was investigated in detail experimentally. The JaVA system in this study is derived from the work of Lachowicz et al., 1999. However, unlike there, we built a larger JaVA system and tested it in still water at much lower frequencies of order one. While attesting the same governing JaVA parameters (e.g. Reynolds number, scaled amplitude), such low-frequency values would allow us real-time observations with naked eye. The typical flow regimes induced by the JaVA system include angled jet, vertical jet, wall jet and vortex flows, as reported by Lachowicz et al., 1999. In this paper, we investigate the detailed quantitative temporal behaviour of basic JaVA-induced flow types utilizing the optical flow concept based on an image-gradient processing method. The temporal dynamics of instantaneous velocity fields obtained via optical flow are then investigated using Fourier analysis.

1 INTRODUCTION

This paper focuses on investigation of the dynamics of a zero-net-mass-flux actuator for active control of boundary layers and flow separation, which is characterized by a high flexibility of operation. This active flow control device, called the Jet and Vortex Actuator, or simply JaVA, is expected to achieve control of drag in boundary layers or re-energize laminar and turbulent boundary layers to resist to separation. For improving aircraft aerodynamic performance, existing flow control strategies have been mostly based on passive control. Passive control means that fixed devices/elements are used to control/intervene the flow. For example, fixed vortex generators often can be

used for passive flow control (Gad-el-Hak, 2006). Conventional passive vortex generators are simple and usually effective to overcome existing flow separation problems (Taylor, 1948). These devices are low cost in manufacture, but they have two significant disadvantages: first, passive flow control devices cannot be optimized for multiple flight conditions (e.g., landing, take-off and manoeuvring), and second, they add an extra drag in steady cruise conditions in which they are no longer needed (Lachowicz et al., 1999). Active flow control, on the other hand, can defeat these disadvantages and optimize overall performance of the flight. Specifically, the jet and vortex actuator (JaVA) would add no or only negligible drag when the system is not actuated and it does not need any external fluid because it is a zero-net-mass flux system.

The JaVA enables to achieve different flow regimes such as angled, vertical and wall jets and vortex flows since it can operate over a range of amplitudes and frequencies. This kind of active flow control includes vortex generation and discrete jet injection for streamwise vortex generation (Wallis and Stuart, 1951). On the other hand, wall jets have been shown to be capable of a straightforward flow separation control which is applied to military fighters (Gratzer, 1971). In another research, it has been shown that active flow control via vorticity generation enhanced boundary-layer momentum transport and thus suppressed stall for both compressible and incompressible flows (Mc Manus et al., 1997). With the full understanding and interaction with boundary layers, a successful application of a JaVA system may lead to efficient flight control systems, thus manoeuvrability, stability and longer aircraft range can be possible at a reduced cost.

2 THE JAVA SYSTEM

Our JaVA body is a Plexiglas cavity with an actuator plate which is moving up and down like a piston and driven by an eccentric tappet like the cam shaft of a car engine. The frequency and the amplitude of the actuator can be changed

by changing the motor speed and the tappet geometry, respectively.

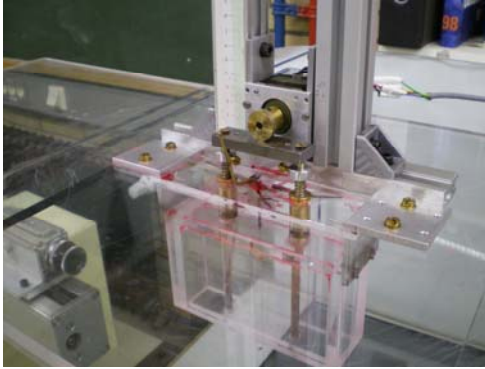


Figure 1a: The JaVA system.

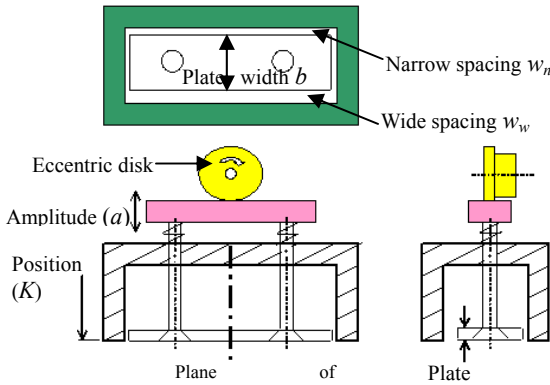


Figure 1b: Schematic views of the JaVA system.

As illustrated in Figure 1b, the actuator plate is placed asymmetrically inside the cavity of the JaVA box, such that there are one narrow and one wide gap between the plate and the box. We have used five plates with various widths and several tappets (i.e. eccentric disks) with various eccentricities designed for our system parameters.

For the current investigations, the actuator plate has a width of $b = 25 \text{ mm}$ (for angled and wall jets) and 26.6 mm (for vortex flow), and it is driven by an eccentric disk with $a = 1.28 \text{ mm}$ eccentricity (i.e., amplitude of actuator plate, from peak-to-peak!). Depending on the wide/narrow slot spacing w_w/w_n , the actuator plate width b , the amplitude a , the frequency f and the relative position of the actuator plate, one can obtain different flow regimes. From these dimensional parameters, Reynolds number ($Re = 2\pi a f b / \nu$) and scaled amplitude ($S_a = 2\pi a / b$) are derived to be able to generalize flow types based on non-dimensional parameters. Additional information about the setup and the influence of other parameters, like the plate position (K) can be found in Gunes et al., 2008.

3 EXTRACTION OF OPTICAL FLOW

Optical flow is an image processing technique for the calculation of velocity fields (Horn & Schunk, 1981). The method computes vector fields from an analysis of the grey-

scale values in consecutive snapshots of a scene. So, under certain restrictions, the velocity field of the observed structures can be faithfully estimated. One restriction includes, for example, that moving elements should have constant brightness over their lifetime for an accurate determination of the optical flow. This assumes that the illumination of the images is homogeneous, and that the light intensity and the brightness of each moving element are constant.

With the optical flow concept the flow velocity of the observed structures can be calculated using the apparent motion of the image. In the following, we employ a gradient-based method for the extraction of the optical flow. In this method, the image intensity, I is given by the brightness constraint equation as follows:

$$I(x, y, t) = I(x + u\delta t, y + v\delta t, t + \delta t) \quad (1)$$

Expanding the right-hand side of equation (1) about the point (x, y, t) in a Taylor series, one gets

$$I(x, y, t) = I(x, y, t) + \delta x \frac{\partial I}{\partial x} + \delta y \frac{\partial I}{\partial y} + \delta t \frac{\partial I}{\partial t} + \varepsilon, \quad (2)$$

where ε contains higher-order terms. In the limit as $\delta t \rightarrow 0$ this equation becomes

$$\frac{dI}{dx}u + \frac{dI}{dy}v + \frac{dI}{dt} = 0. \quad (3)$$

Equation (3) cannot be solved for a single point in the image so some constraints are to be applied. One common constraint is to assume that in a small neighborhood the velocity vector (optical flow) is constant. By combining the pixels in the neighborhood we obtain an over-determined system of equations (Burkhardt and Bredebusch, 1994),

$$\begin{bmatrix} \frac{dI}{dx}(1,1) & \frac{dI}{dy}(1,1) \\ \frac{dI}{dx}(1,2) & \frac{dI}{dy}(1,2) \\ \vdots & \vdots \\ \frac{dI}{dx}(N_1, N_2) & \frac{dI}{dy}(N_1, N_2) \end{bmatrix} \begin{bmatrix} u \\ v \end{bmatrix} = \begin{bmatrix} -\frac{dI}{dt}(1,1) \\ -\frac{dI}{dt}(1,2) \\ \vdots \\ -\frac{dI}{dt}(N_1, N_2) \end{bmatrix} \quad (4)$$

The system in equation (4) can be solved using a least-squares based pseudo-inverse method.

In equation (4), N_1 and N_2 denote the number of pixels in each spatial direction for a selected sub-region. Note that in a sub-region containing $(N_1 \times N_2)$ pixels, there is a single, unique velocity vector. Selection of a too small sub-region causes insufficient smoothing which leads to noise while a too big sub-region causes too much averaging and hence low resolution.

4 TYPICAL FLOW REGIMES

4.1 Angled Free Jet Flow at $f = 1$ Hz

For seeding of the flow the actuator cavity has been filled with fluorescent dye which starts to mix with the external flow when the actuator runs. Figure 2a shows typical snapshots in a given periodic cycle of angled free jet flow visualizations obtained by an image acquisition system consisting of a visualization laser and a fast camera. Due to the low forcing frequencies (e.g., 1 Hz), 30 or 60 frames per second (*fps*) were sufficient to identify the dynamic characteristics of the flow. For such rather low *fps* values, relatively long visualization image series can be recorded which allowed further detailed temporal analyses. Figure 2b

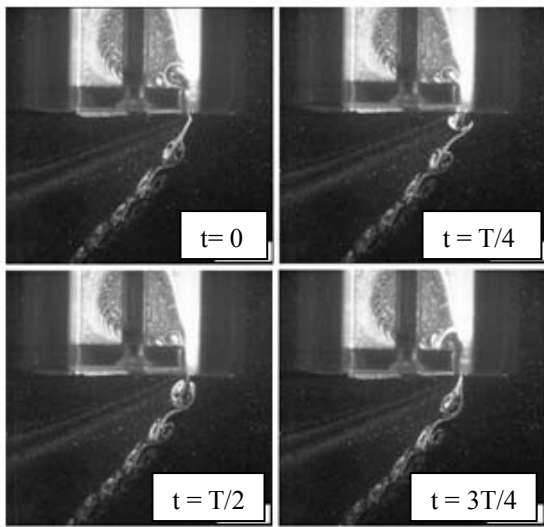


Figure 2a: Snapshots (equally spaced over one cycle, $f = 1$ Hz, $Re = 201$, $S_a = 0.32$)

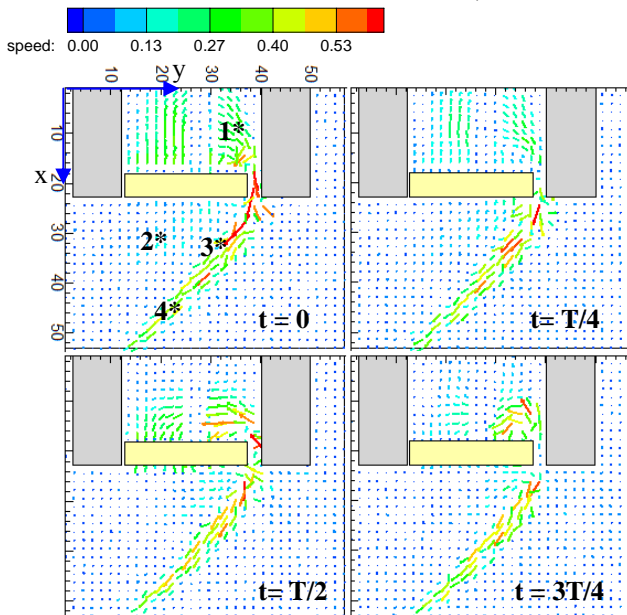


Figure 2b: Instantaneous velocity magnitude fields of the free angled jet in figure 2a.

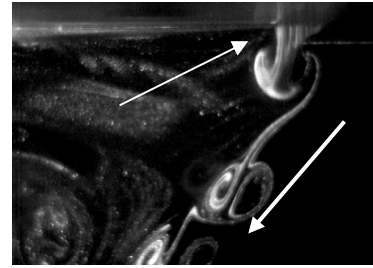


Figure 3a: Close-up of snapshot at $t = T/4$.

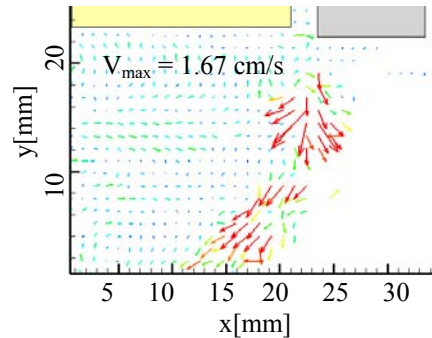


Figure 3b: Close-up of optical flow at $t = T/4$

gives the corresponding optical flow fields obtained from the grey-scale images of Fig. 2a.

Figure 3a and 3b show a close-up of the snapshot at time $t = T/4$ and corresponding optical flow during ejection of the fluid from the wide gap. The fluid ejection occurs when the plate moves upward due to the incompressibility so the mean flow speed at the wide gap during the ejection is calculated to be 2.56 cm/s. In figure 3a, we also denote the flow directions in that the repeating packets of fluid is ‘pumped’ out of the cavity with the plate frequency, and there is an almost continuous flow into the cavity at the wide gap in order to fulfil the zero-net-mass flow of the JaVA system. Here it should be noted that the present flow regime is not expected to energize a prospective boundary layer in the most efficient way, because of the reverse flow (i.e. the upper arrow in Fig. 3a) that occurs at the same time as the angled jet but which runs into opposite direction to the jet.

In order to characterise the dynamical behaviour of the angled jet shown in Figure 2 in quantitative manner, we performed FFT analyses at four representative points (their locations are marked with 1, 2, 3, and 4 on the first snapshot). We had a total of 500 optical-flow snapshots extracted from visualization images (amounting approximately to a signal length of 17 cycles with 30 *fps*). This data is shown as red dots in the time history plots of velocity components u_i , v_i in x - and y -directions, respectively at points 1-4 in Figure 3a-d. Note, that u is oriented in *downward* direction, in accordance with the x , y coordinates defined in Figure 2b. Before investigating the frequency spectrum of the flow, we interpolate these data onto 4096 points (power of 2) by line Kriging (blue solid line) prior to FFT analysis. Kriging interpolation is known to be an optimal statistical estimation procedure. It uses weighted

linear combinations of the available data and estimates unknown values from data observed at known locations (see Gunes and Rist (2007) and Davis (2002) for details). The frequency spectrum obtained by FFT shows a single frequency with higher harmonics.

The angled jet flow, for $Re = 201$, $S_a = 0.32$, is periodic with peak amplitude at $f = 1.02 \text{ Hz}$. The frequency is very close to the input frequency as expected and validates the accuracy of the optical flow fields calculated.

As it can be seen from Figures 4a-d, for all points, the basic dynamic characteristics of the flow is the same, i.e., the flow oscillates with a single frequency of $f = 1 \text{ Hz}$. However, at points close to the actuator plate (points 1 and 3), the frequency amplitude is strong for both components of velocity. On the other hand, while the peak frequency is still noticeable at $f = 1 \text{ Hz}$ for points 2 and 4, it is very small (in the noise range of the spectrum of point 3).

In addition, it can be seen very clearly, for point 2 (outside the active jet flow), that the x -velocity component is clearly periodic but the y -component has a noisy low-frequency oscillation. This can be explained with the fact that there is mainly a horizontal flow along the actuator plate's surface

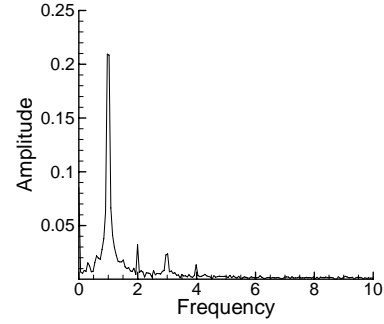
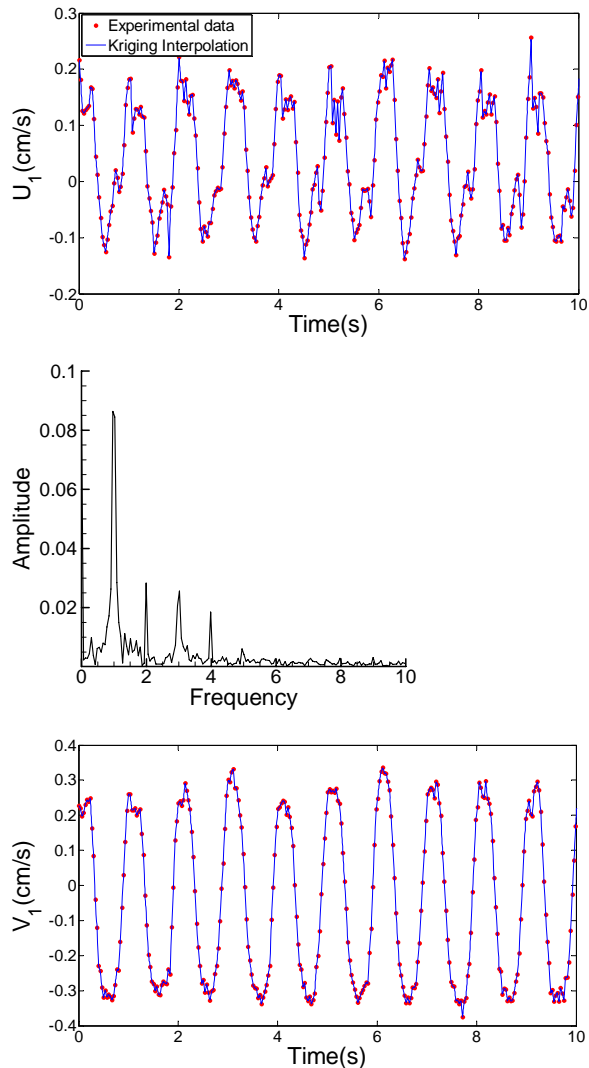


Figure 4a: Time history and frequency spectra of an angled jet (Point 1: $x = 11.0$, $y = 35.2$, $f = 1 \text{ Hz}$, $b = 25 \text{ mm}$).

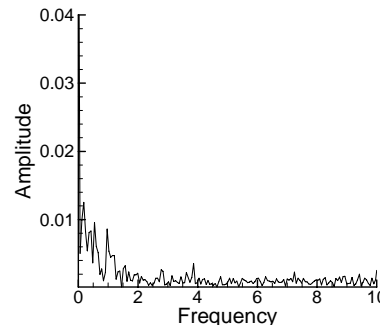
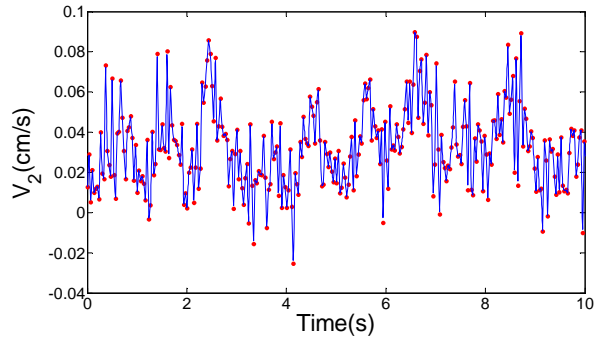
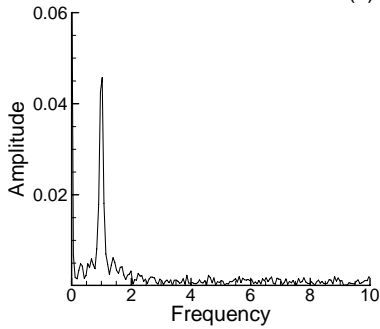
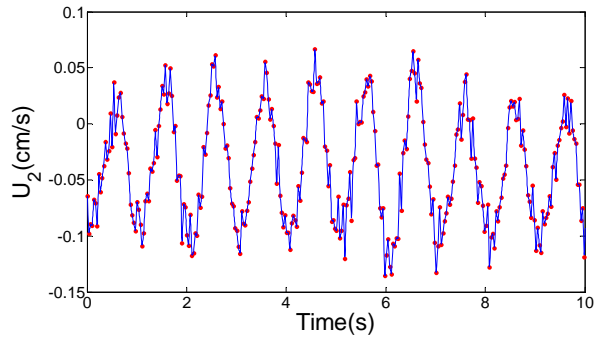


Figure 4b: Time history and frequency spectra of angled jet (Point 2: $x = 29.5$, $y = 20.7$, $f = 1 \text{ Hz}$, $b = 25 \text{ mm}$).

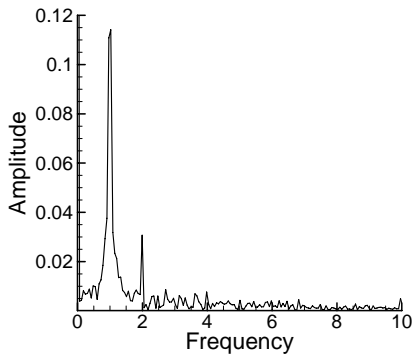
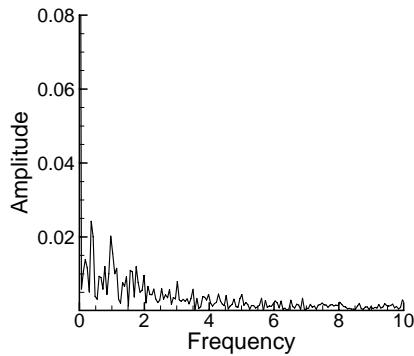
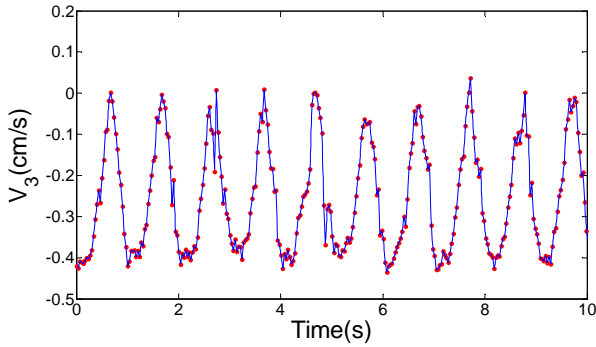
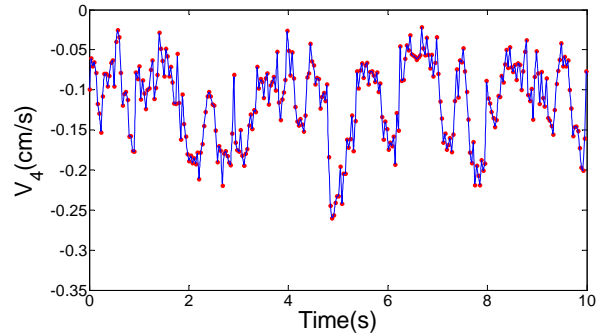
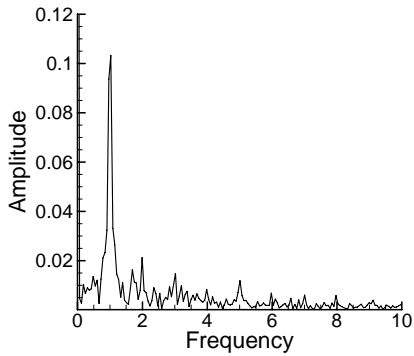
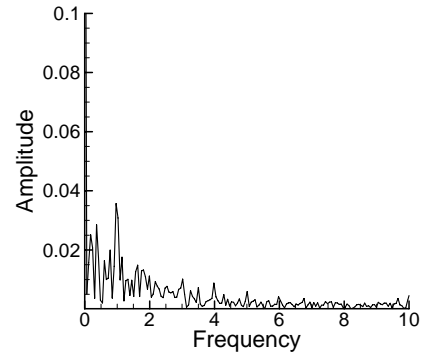
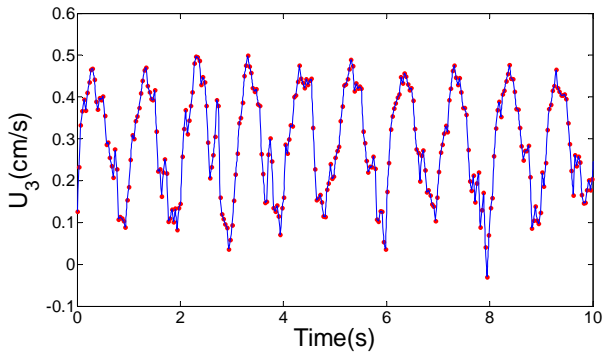


Figure 4c: Time history and frequency spectra of angled jet (Point 3; $x = 31.2$, $y = 33.4$, $f = 1$ Hz, $b = 25$ mm).

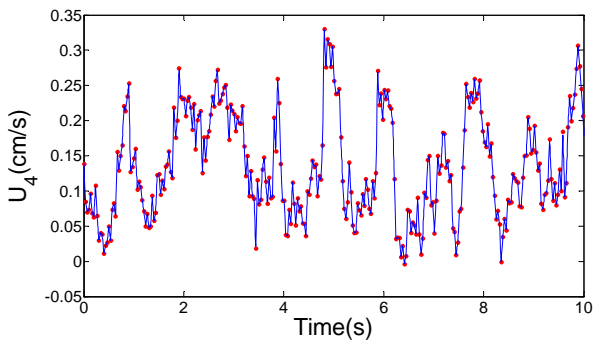


Figure 4d: Time history and frequency spectra of angled jet (Point 4; $x = 44.7$, $y = 26.2$, $f = 1$ Hz, $b = 25$ mm).

towards the wide gap (see Fig. 3a). A similar noisy signal is observed downstream of the jet as depicted with point 4. We note that between points 3 and 4 the free jet flow speed is reduced more than 50 % in magnitude as shown in figures 4c and 4d.

4.2 Wall Jet Flow at $f = 2$ Hz

We have mentioned that different flow regimes can be achieved by changing various governing parameters such as the frequency of the oscillating plate, the amplitude of the eccentric plate, mean position of the actuator plates and wide and narrow gap widths. In this section, we present results for a wall jet in Figure 5a, which shows a typical instantaneous visualization snapshot at $f = 2$ Hz. Except for the plate frequency (that is, Reynolds number), all the other governing parameters are kept the same as in the previous free (angled) jet flow. Temporal visualization results (motion pictures) show that there is a strong periodic (2 Hz) fluid ejection from the wide gap which results in a quasi-steady flow along the actuator's plate towards the left as

indicated in figure 5a. It is also apparent that additional fluid is trapped into the wall jet (left) flow increasing the momentum flux of the wall jet downstream. On the other hand, since the JaVA is a zero-net-mass flow device, there is a continuous flow suction from the right side of the wide gap to compensate the ejected fluid. The arrows illustrate the observed flow directions in figure 5a. Similar to the angled jet in the previous section, we extracted a total of 500 snapshots for optical flow-field extraction for the wall jet from which we show an instantaneous field in figure 5b. Then, we obtained the time histories and corresponding frequency spectra for the selected points which are shown in Fig. 5b.

Inside the cavity and just outside of the wide gap the flow is found to be periodic (2 Hz) as reflected by FFT results in figure 6a. On the other hand, downstream of the wall jet the flow loses its periodicity and becomes rather chaotic as shown in figure 6b. The time history plots (figure 6a and 6b) show that, while the vertical velocity component u decreases along the main flow direction, the horizontal velocity component (the main flow) increases. Therefore, this flow regime can potentially be used to energize a prospective boundary layer outside of the actuator.

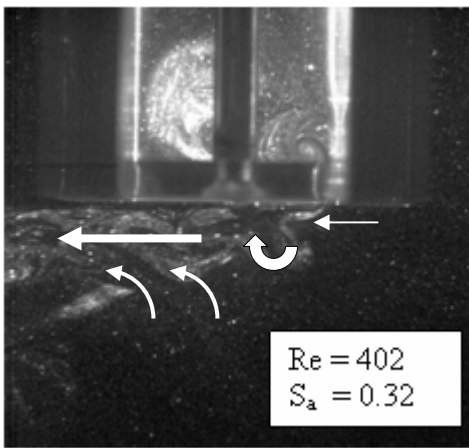


Figure 5a: Instantaneous snapshot of a wall jet ($f = 2 \text{ Hz}$, $Re = 402$, $S_a = 0.32$)

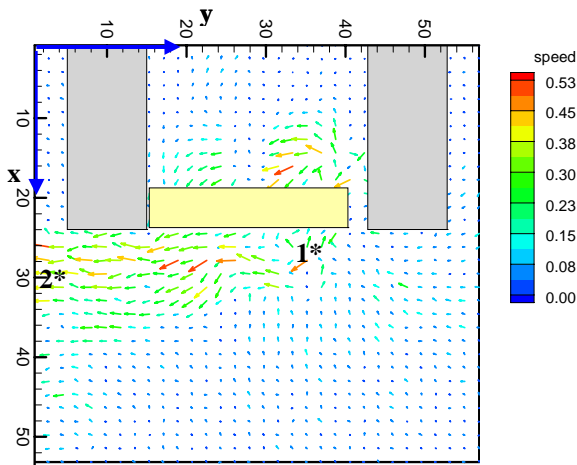


Figure 5b: Instantaneous velocity magnitude field (in cm/s) of the wall jet case ($f = 2 \text{ Hz}$, $Re = 402$, $S_a = 0.32$)

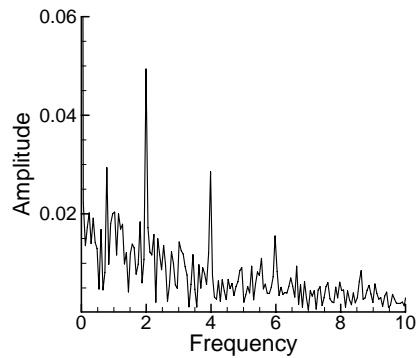
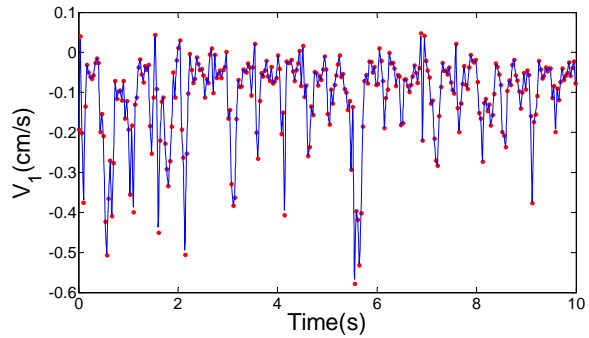
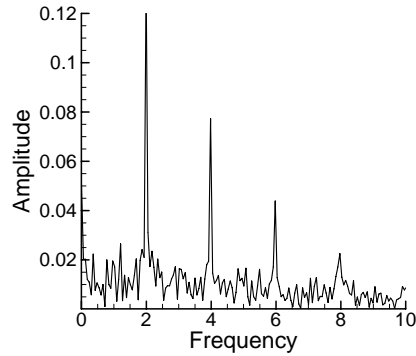
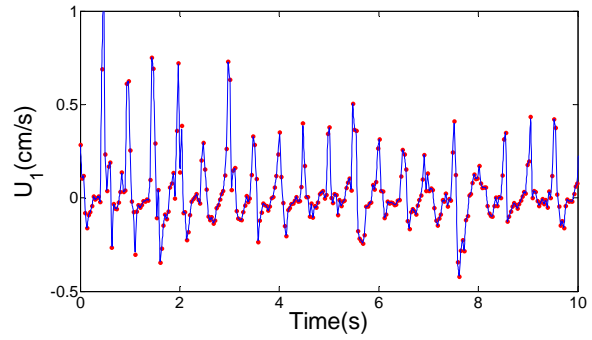


Figure 6a: Time history and frequency spectra of wall jet (Point 2: $x = 27.8$, $y = 38.8$, $f = 2 \text{ Hz}$, $b = 25 \text{ mm}$).

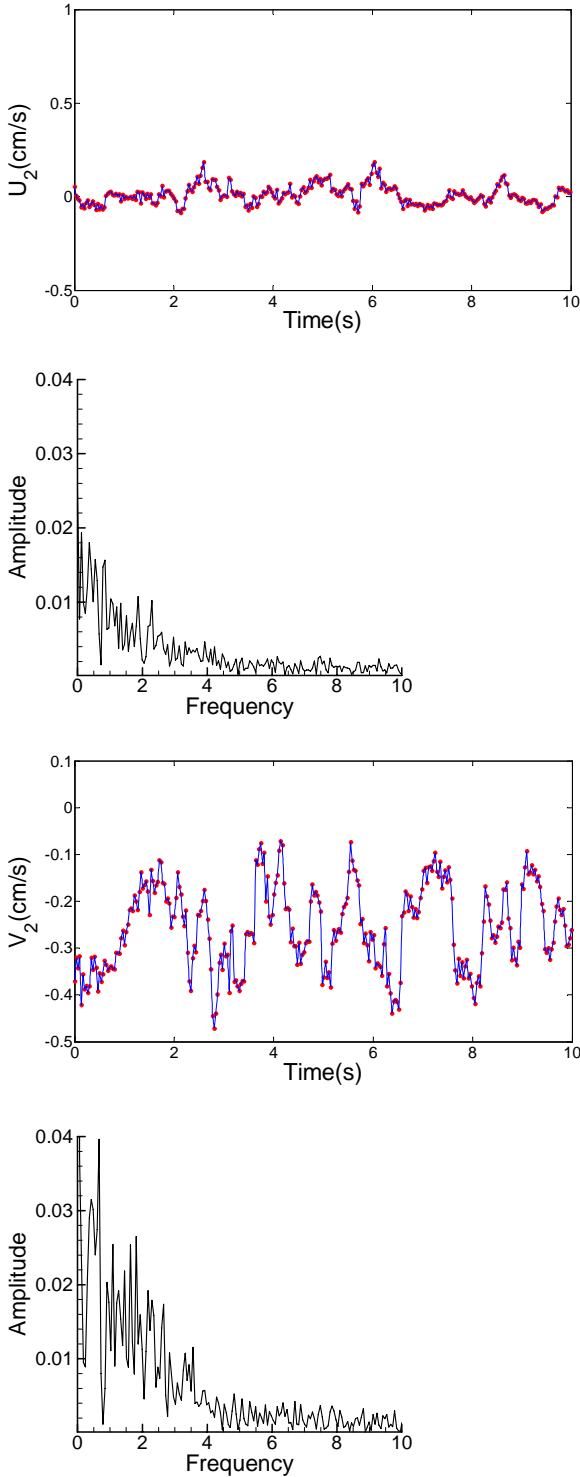


Figure 6b: Time history and frequency spectra of wall jet
 (Point 4: $x = 29.5$, $y = 2.7$, $f = 2$ Hz, $b = 25$ mm).

4.3 Vortex Flow at $f = 1$ Hz ($b = 26.6$ mm)

A vortex flow regime occurs at a frequency of $f = 1$ Hz and plate width of $b = 26.6$ mm (smaller wide gap). As the plate width is changed, both Reynolds number and scaled amplitude S_a change slightly but this has only negligible effect. The main difference from the previous cases is that the average flow speed from the wide gap is increased almost three times compared to the free angled jet as the

wide gap is reduced from 2.5 mm to 0.9 mm. The instantaneous snapshot of a vortex flow is shown in Fig. 7a. It has been observed that the wide gap width is the dominant factor for achieving vortex flow. Due to the high unsteadiness of the flow, for this case, the visualization images are acquired at a frame rate of 60 fps. This, in turn, reduced the total recording time for the instantaneous flow to approximately 8 seconds, which reduced the frequency resolution of the analysis. The location of time history points is denoted in Figure 7b where we illustrate the optical flow field. The selected points are located on and around the clockwise vortex.

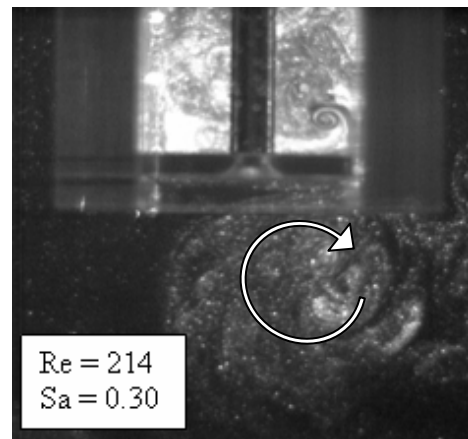


Figure 7a: Instantaneous snapshot of a vortex flow
 ($f = 1$ Hz, $b = 26.6$ mm)

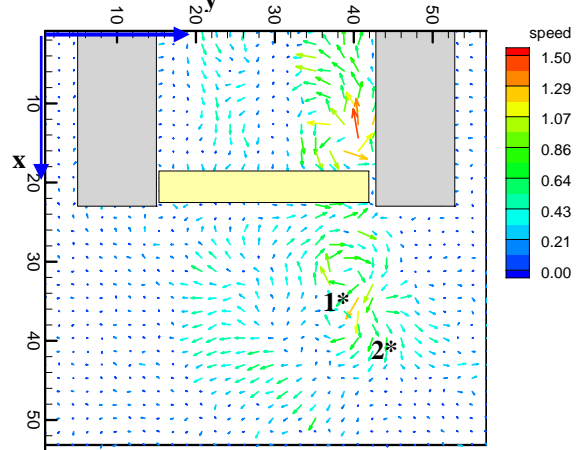


Figure 7b: Instantaneous velocity magnitude field (in cm/s)
 of the vortex flow ($f = 1$ Hz, $b = 26.6$ mm)

For a given frequency and amplitude of the JaVA system, as the width of the wide gap decreases (or the plate length increases) the flow becomes more complicated due to higher local speeds at/around the wide gap, and the flow becomes unsteady. For the selected case, we observed an unsteady vortex flow rotating in clockwise direction. Time histories and their spectra shown in Fig. 8a-b confirm that the flow is unsteady both in- and outside of the JaVA.

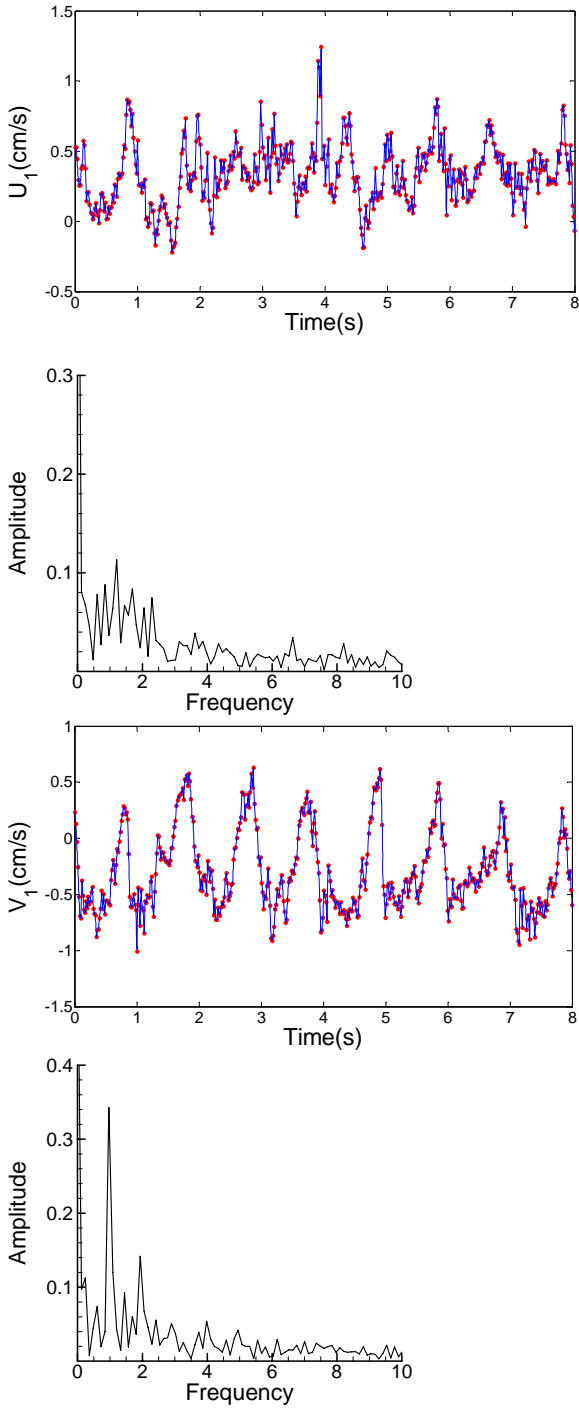


Figure 8a: Time history and frequency spectra of vortex flow (Point 1: $x = 35$, $y = 38.8$, $f = 1$ Hz, $b = 26.6$ mm).

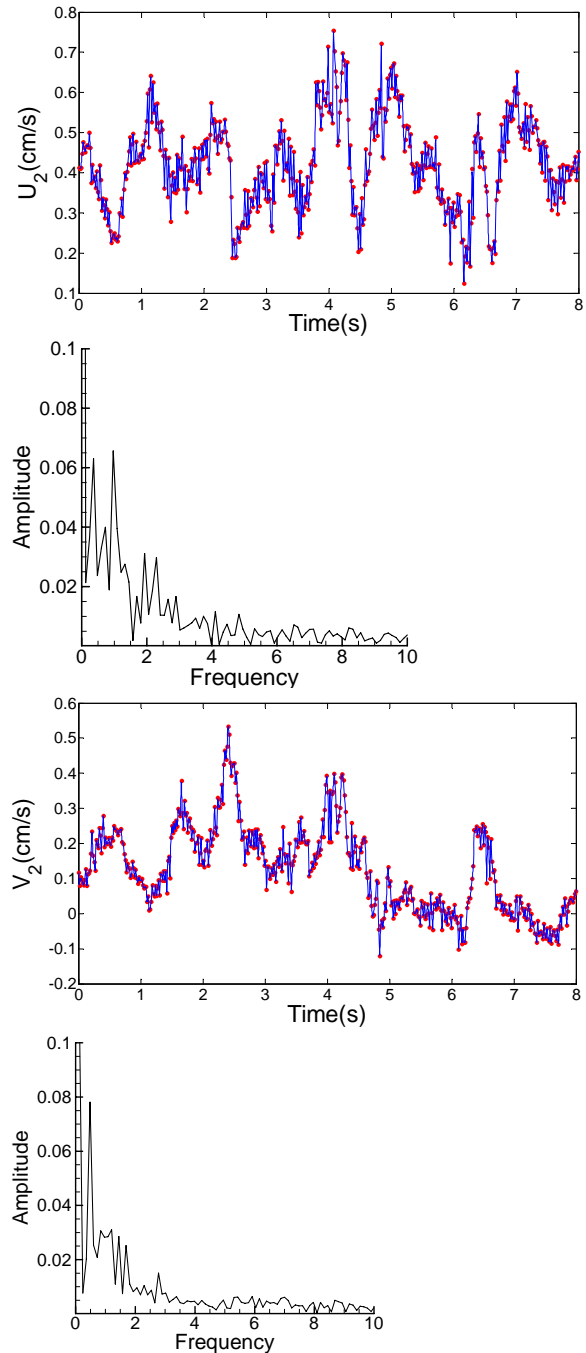


Figure 8b: Time history and frequency spectra of vortex flow (Point 2: $x = 39.7$, $y = 46$, $f = 1$ Hz, $b = 26.6$ mm).

Finally, we present time-averaged flow visualizations and corresponding optical flow fields for comparison of the different flow regimes in figure 9. The vortex flow produces the largest velocity magnitude as it has an average fluid ejection speed of 7.5 cm/s from the wide gap. Compared to the free angled and the wall jets, we find another interesting result: Even if the average fluid ejection speed from the wide gap is twice as large for the wall jet due to the doubling of the frequency (approximately 5 cm/s), its averaged maxi-

imum flow velocity is smaller than that of the free angled jet. This could be due to the presence of the oscillating wall along which the horizontal jet flows. It is believed that apart from the maximum speeds the ejection and suction flow directions are important if one wants to use this type of actuator to increase the fluid momentum along the external wall. The interaction and robustness of the observed flow regimes with the boundary layer developing along such a wall is also important for the selection of an appropriate JaVA flow regime.

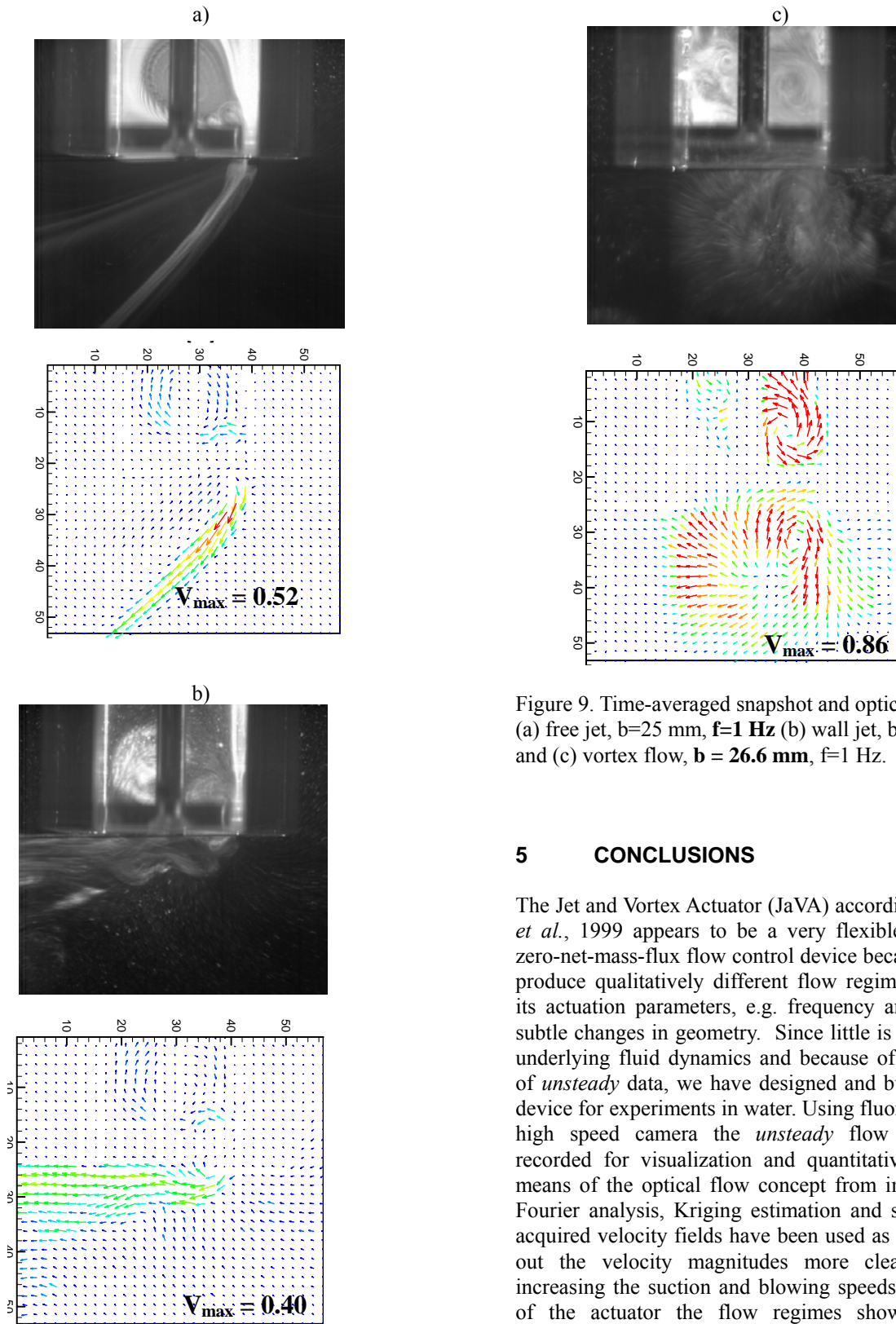


Figure 9. Time-averaged snapshot and optical flow field for (a) free jet, $b=25$ mm, $f=1$ Hz (b) wall jet, $b=25$ mm, $f=2$ Hz and (c) vortex flow, $b = 26.6$ mm, $f=1$ Hz.

5 CONCLUSIONS

The Jet and Vortex Actuator (JaVA) according to Lachowicz *et al.*, 1999 appears to be a very flexible and interesting zero-net-mass-flux flow control device because it appears to produce qualitatively different flow regimes depending on its actuation parameters, e.g. frequency and amplitude, or subtle changes in geometry. Since little is known about the underlying fluid dynamics and because of a complete lack of *unsteady* data, we have designed and built an according device for experiments in water. Using fluorescent dye and a high speed camera the *unsteady* flow field has been recorded for visualization and quantitative evaluation by means of the optical flow concept from image processing. Fourier analysis, Kriging estimation and smoothing of the acquired velocity fields have been used as well. This brings out the velocity magnitudes more clearly. Thus, by increasing the suction and blowing speeds through the gap of the actuator the flow regimes shown underwent a transition from an oblique jet through a wall jet to a vortex mode. Thus, all qualitative features described by Lachowicz *et al.* 1999 have been reproduced but our results are much more detailed and consist of instantaneous velocity fields for quantitative analysis. It has been observed that wall jet and vortex flow can be potentially useful to increase the momentum of the flow in an external boundary layer.

According research is under way to test the performance of the JaVA-induced flows to control a boundary layer flow.

Acknowledgements

We gratefully acknowledge the financial support of Scientific and Technical Research Council of Turkey (TÜBİTAK) and International Bureau of the Federal Ministry of Education and Research (BMBF), Germany through the project "Development and Testing of a Jet and Vortex Actuator (JaVA) for Active Flow Control", Nr. 107M644 and TUR 07/006, respectively.

References

- Burkhardt, H and Bredebusch, A. "Application of digital image processing methods for the analysis of local structures in fluidized bed processes". Research project C8, 1994.
- Davis, J.C., "Statistics and data analysis in Geology", New York, J. Wiley, 2002.
- Gad-el-Hak M., Flow Control- Passive, Active and Reactive Flow Management. Cambridge University Press, 2006.
- Gratzer L. B., "Analysis of Transport Applications for High Lift Schemes" AGARD- LS- 43-71, Paper No:7, Rhode Saint Genese, Belgium, 1971.
- Gunes, H., Cadirci, S., and Rist, U. "An Experimental Investigation of Jet and Vortex Actuator for Active Flow Control", AIAA 2008-3761, 4th Flow Control Conference and Exhibit 23-26 June 2008, Seattle, WA.
- Gunes, H. and Rist, U. "Spatial resolution enhancement / smoothing of stereo-particle-image-velocimetry data using proper-orthogonal-decomposition-based and Kriging interpolation methods" Physics of Fluids 19 (6): Art. No. 064101, 2007.
- Horn B. K. P., Schunck B. G. "Determining optical flow", Artificial Intelligence, 17, 1981, 185-203.
- Lachowicz J. T., Yao C., Wlezien R. W., "Flow field characterization of a jet and vortex actuator", Experiments in Fluids, 27, 1999, 12 – 20.
- Mc Manus K. and Magill J. "Separation Control in Incompressible and Compressible Flows Using Pulsed Jets", AIAA Paper No. 97, Washington D.C., 1971.
- Taylor, H. D., "Application of Vortex Generator Mixing Principles to Diffusers", Research Department Concluding Report No. R- 15064-5, United Aircraft Corporation, Connecticut, 1948.
- Wallis R. A., and Stuart C. M., "On the Control of Shock Induced Boundary Layer Separation with Discrete Jets", Aeronautical Research Council Current Paper No. 494, London, Great Britain, 1958.